Design of a Liquid Crystal based sensor for Dopamine detection

Lisha Loitongbam
(MS13061)

A dissertation submitted for the partial fulfilment of
BS-MS dual degree in Science

Indian Institute of Science Education and Research Mohali
April 2018

Certificate of Examination

This is to certify that the dissertation titled "**Design of a liquid crystal based sensor for dopamine detection"** submitted by **Ms. Lisha Loitongbam** (Reg. No. MS13061) for the partial fulfilment of BS-MS dual degree programme of the institute, has been examined by the thesis committee duly appointed by the institute. The committee finds the work done by the candidate satisfactory and recommends that the report be accepted.

Dr. Sugumar Venkataramani

Dr. Debashis Adhikari

Dr. Santanu Kumar Pal
(Supervisor)

Dated: April 20, 2018

Declaration

The work presented in this dissertation has been carried out by me under the guidance of Dr. Santanu Kumar Pal at the Indian Institute of Science Education and Research Mohali. This work has not been submitted in part or in full for a degree, a diploma, or a fellowship to any other university or institute. Whenever contributions of others are involved, every effort is made to indicate this clearly, with due acknowledgement of collaborative research and discussions. This thesis is a bonafide record of original work done by me and all sources listed within have been detailed in the bibliography.

Lisha Loitongbam
(Candidate)

Dated: April 20, 2018

In my capacity as the supervisor of the candidate's project work, I certify that the above statements by the candidate are true to the best of my knowledge.

Dr. Santanu Kumar Pal
(Supervisor)

Acknowledgement

Firstly, I would like to express my deepest gratitude and regards to Dr. Santanu Kumar Pal, Associate Professor, Department of Chemical Science, Indian Institute of Science Education and Research Mohali for giving me the opportunity to work under his guidance. I am grateful for his advice and suggestions during the course of this thesis.

I would like to thank Dr. Debi Prasad Sarkar, Director, Indian Institute of Science Education and Research Mohali and Dr. A. Babu, Head of Department of Chemical Science as well as Prof. N. Satyamurthy, former Director, Indian Institute of Science Education and Research Mohali and Prof. K.S. Vishwanathan, former Head of Department of Chemical Sciences for authorizing the use of various facilities necessary for this project.

I express my regards to my thesis committee members, Dr.Sugumar V. and Dr. Debashis Adhikari, for providing their valuable feedback and suggestions in the project review meetings.

I express my sincere regards and thanks to Dr. Rajib Nandi, Post doctoral fellow, for guiding me throughout this project and teaching me about the system from scratch. I am extremely grateful to him for his patience and advice during this research project.

I would also like to thank the PhD scholars: Ipsita , Joydip , Indu Bala, Indu Verma, Shruti, Yogi, Dibyendu, Dr. Monika, Vidhika , Supreet and Varsha and post doctoral fellows: Dr. Rajib Nandi, Dr. Golam, Dr. Manisha, Dr. Nazma and Dr. Subrato for their cooperation and companionship in the lab. I am deeply grateful to my classmates: Vaishnavi S., Nitya Singh, Neelima P.R. and Swathy Lekshmy V.S. for always being supportive and ready to lend a hand.

Finally, I express my love and regards to my family and friends for their unwavering support and encouragement.

Lisha Loitongbam

List of Figures

List of Schemes

Abbreviations

LC	Liquid Crystal
OTS	Octadecyltrichlorosilane
DMOAP	N,N-Dimethyl –N- octadecyl-3-aminopropyltrimethoxysilyl chloride
POM	Polarizing Optical Microscope
SERS	Surface Enhanced Raman Spectroscopy
5CB	4-cyano-4'-n-pentylbiphenyl
GNP	Gold nanoparticles
UV-Vis-NIR	Ultraviolet- Visible-Near Infra Red
FT-IR	Fourier Transform Infra Red
TEM	Transmission Electron microscope
DCM	Dichloromethane
Tof MS	Time of flight Mass Spectrometer
MALDI	Matrix Assisted Laser Desorption/ Ionization
NMR	Nuclear Magnetic Resonance
DLS	Dynamic Light Scattering
DSP	Dithiobis(succinimidylpropionate)
PBS	Phosphate Buffer Saline
3-PBA	3-Pyridinium Boronic Acid
NHS	N-hydroxysuccinamide

Contents

Abstract

Dopamine is an important neurotransmitter and its abnormal levels are associated with a variety of mental disorders. Considering the importance of this molecule, we designed a sensor for dopamine using a boronic acid based amphiphile to align the LC film. The boronic acid head group of the amphiphile interacts with the cis diol of dopamine , thus disrupting the LC interface resulting in appearance of bright appearance under cross polars. We have designed a system consisting of two point selective sites by exploiting the amine group of dopamine as the cis diol interaction with boronic acid is not very specific. This was linked with an amine selective crosslinker dithio(bissuccinimidylpropionate) which was functionalized on a GNP. This, in turn, disrupts the LC alignment more creating an enhancement in optical signals

Chapter 1 deals with the basics of liquid crystals and its properties which are responsible for its application in biosensors. Descriptions of dopamine and the formation of cyclic boronate esters from interactions of boronic acids and cis diols are given in this chapter

Chapter 2 talks about the materials used and experimental protocols adopted in designing the sensor.

The results and conclusions derived from the project are discussed in Chapter 3.

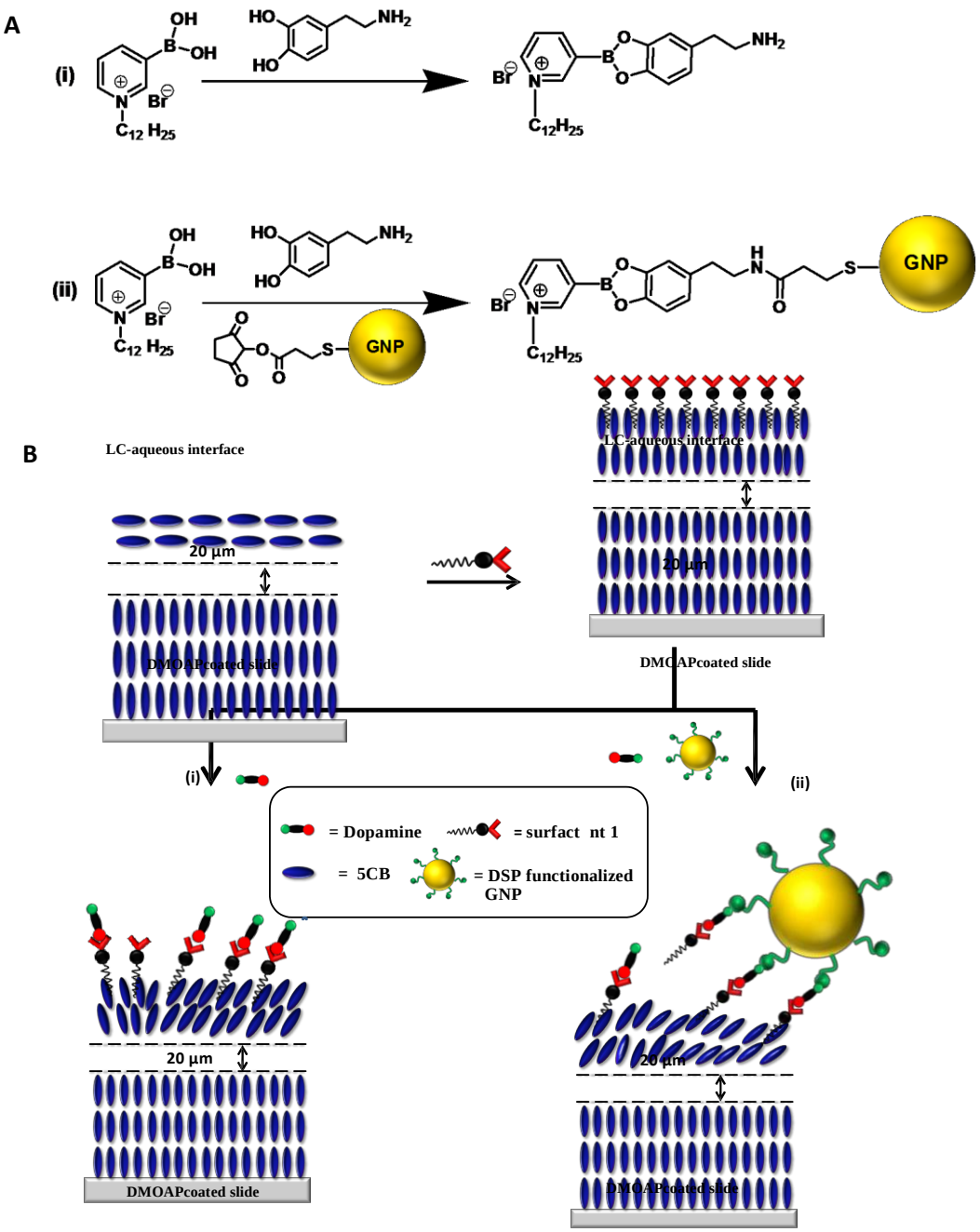

Scheme 1: Schematic diagram for dopamine detection: **A** (i) formation of cyclic boronate ester on interaction of dopamine and surfactant 1 (ii) linking of surfactant 1-dopamine complex with DSP functionalized GNP through amide bond formation; **B** Changes in alignment of 5CB films in aqueous media and surfactant solution; (i) and (ii) shows changes in alignment of 5CB on interaction with complexes A (i) and (ii) respectively.

Chapter 1

Introduction

1.1 Liquid crystals (LCs)

Liquid crystals are molecules showing properties which are intermediate to isotropic liquids and crystalline solids. [1-4] LCs have anisotropic material properties such as refractive index, elasticity, viscosity, birefringence, response to electric and magnetic fields. They possess long range orientational order with some degree of rotational order and partial translational order; despite the absence of a lattice. This partial ordering in the bulk results in the formation of an 'ordered fluid phase. [4] LCs form mesophases, the transitional phase between ordered phases with long range order in all directions and the disordered phase in which molecules can explore all possible orientations.[1-4] The molecules forming liquid crystals , called mesogens, are usually anisotropic in shape ; however isotropic molecules can be driven to self assemble leading to the formation of anisometric units with interactions such as hydrogen bonding, π- π interactions, etc.[5] The averaged direction of orientation of LCs is known as the director.

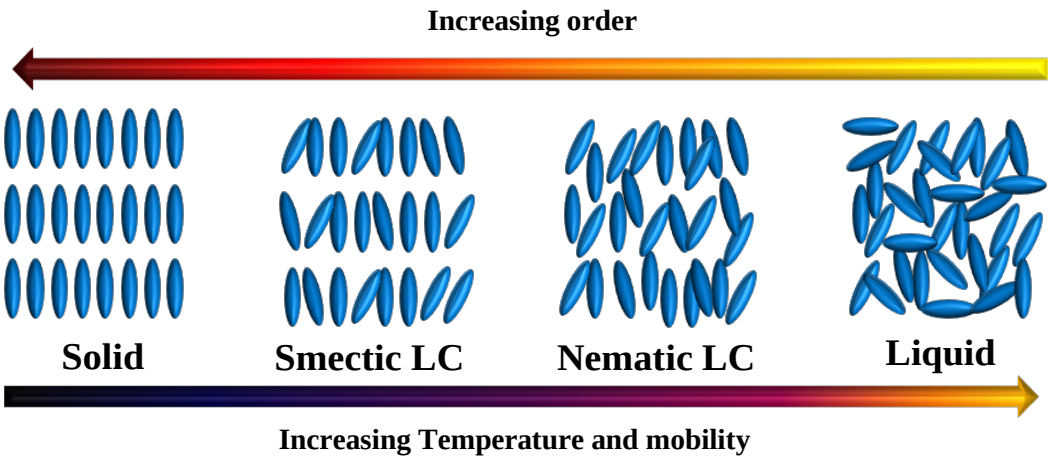

Figure 1: Illustration showing that liquid crystalline phase exist between crystalline solid and isotropic liquid

1.2 History of LCs

The discovery of liquid crystals is credited to Freidrich Reinitzer; an Austrian botanist working in the Institute of Plant Physiology, University of Prague; studying the role of cholesterol in plants. In 1888, Reinitzer came across an organic molecule derived from cholesterol (cholesterol benzoate) which was found to have two melting points : 145.5^0C to a cloudy liquid and a clear liquid at 178.5^0C.[3] Reinitzer approached a German physicist, Otto van Lehmann, who was studying the crystallinity of compounds using a polarizing microscope with a heating stage.

Lehmann noted the similarities between cholesteryl benzoate and some of the other compounds he observed previously and was convinced of an existence of an order different from the conventionally known states of matter, possessing properties similar to that of both solids and liquids. He termed this class of compounds as crystalline liquids or soft solids. Though their findings were repeatedly challenged by other scientists who believed that their sample was simply a mixture of different compounds, the existences of these LC phases were supported through several experiments and theories in the 1910-1930s.

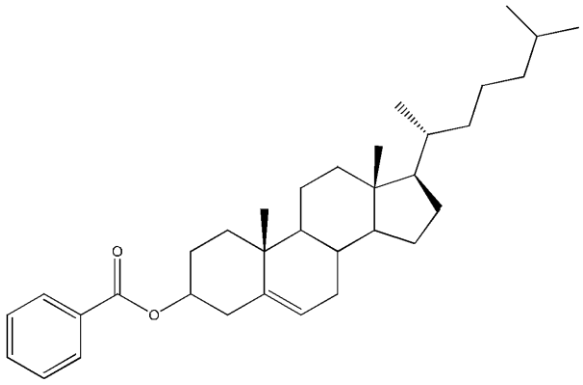

Figure 2: Structure of Cholesteryl benzoate

1.3 Nematic mesophase

Nematic mesophase is the simplest phase of LCs and is observed in calamitic (rod like) and discotic (disc like) molecules. It is the least ordered phase, possessing only one degree of order. The nematic mesophase has thread-like appearances when observed under the polarizing optical

microscope, arising from presence of defects in orientational order known as disclinations in which the direction of orientation is undefined .[2]

The arrangement of molecules in the nematic mesophase is disordered with respect to each other but owing to its shape anisotropy; the averaged direction of the long molecular axes of the molecules orient towards a preferred direction called the director n (r). The direction of n (r) can be arbitrary in space. The director of the nematic mesophase is a unit vector as the magnitude and the sign of the vector has no physical significance, i.e. the n and −n states are indistinguishable because there is no preferred ordering of molecules of the two ends of the long

axis as the molecule may rotate along their long axis.[6] Thus, the nematic mesophase has a long range orientational order and lacks a long range positional order in space. Nematic mesophase is a uniaxial medium and all its optical properties of the nematic mesophase are defined with

respect to the the director n(r) as the properties along $n_{\perp}$ are different from $n_{\parallel}$.

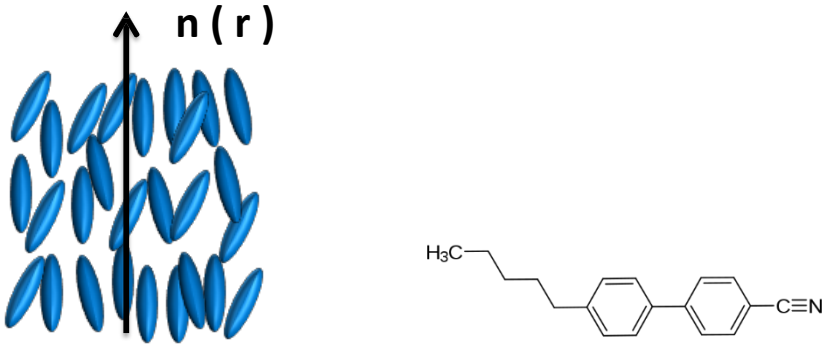

Figure 3: A) Illustration of the nematic LC aligned along the director B) nematic 5CB

The degree of orientational order of the mesophase is represented by the order parameter S (Equation 1.1). It is defined by the average of the second Legendre polynomial. The angle between the director and axis of one molecule is the phase is represented by θ. Value of S for a completely disordered isotropic liquid is zero and an ordered crystalline solid has a value of one.

Usually, S lies in between 0.3 and 0.8 for liquid crystal samples. [2,7]

(Equation 1.1)

The director of the nematic mesophase is very responsive to electric and magnetic fields as well as suitably modified surfaces. Hence, due to its high fluidity and response to fields; nematic liquid crystals are widely used in display devices.[5,6]

This thesis involves the use of the nematic LC 5CB (4-cyano-4′-n-pentylbiphenyl) to study interfacial interactions (figure 3 B). 5CB shows nematic phase between 18^0C and 35^0C but is crystalline at temperatures less than 18^0C and liquid beyond 35^0C.

1.4 Properties of LCs

1.4.1 Surface anchoring

The interaction of LCs with the surfaces of the confining medium influences their orientational ordering. LCs prefer to orient themselves along a direction with lowest free energy. This orientation of the director is known as the easy axis (figure 4).

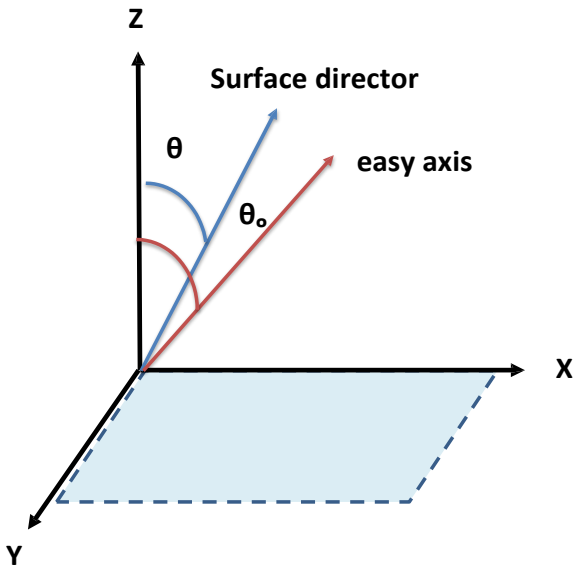

Figure 4: Orientation of the easy axis and surface director on an interface in XY plane

The energetics dependent on surface induced ordering is defined according to the deviation of the director from the easy axis under the influence of external fields.[8]

Equation 1.2 represents the surface dependent orientation energy.

(Equation 1.2)

Where σ and σ_o represents the interfacial free energy and orientation independent component of interfacial free energy, W_a represents the anchoring energy and the orientations of easy axis and surface director is represented by θ_o and θ respectively. [8] The order of orientation independent surface energy part is usually about 10^{-3}-10^{-2} mJ/m^2. Orientational transitions of liquid crystals are caused by changes in energetics of this order, in cases of changes in surface interactions of LCs.[7] As a consequence of LCs possessing long range orientational order, subtle changes in surface interactions leads to ordering transitions over a distance of 100 μm from interfaces. This property is exploited to amplify surface interactions detectable by optical and electronic methods.[8,9]

1.4.2 Elasticity of LCs

The elasticity of the LCs is brought about by its molecular ordering. In a LC phase, the mesogens are assumed to be aligned along a preferred direction represented by a unit vector n (r) called the director. However, this assumption does not hold in most cases as there exists a change in director n(r) orientation with the spatial variation. The distortions in the liquid crystalline phase can be of three types: splay, twist and bend.

Figure 5: Distortions in LC phase : a) twist b) splay c) bend

The elastic free energy per unit volume is given by the Frank- Oseen equation.[2,4,7,8]

(Equation 1.3)

The constants K_{11}, K_{22} and K_{33} represent the elastic moduli of splay, twist and bend configurations and n represents the director of the nematic liquid crystals. The order of magnitude for K_{ii} (modulus of deformation) is approximately 10^{-11} N.

1.4.3 Birefringence

Birefringence is a property of a material in which its refractive indices vary with change in direction of propagation and polarization. This phenomenon is observed in both uniaxial and biaxial anisotropic materials. The refractive indices for light parallel to the director and perpendicular to the director are denoted by $n_{\perp}$ and $n_{\parallel}$ respectively. For the uniaxial nematic LCs; the index of refraction for light polarized in one particular direction that is different from the other two is called the extraordinary index n_e while the refractive index for light polarized perpendicular to it is the ordinary index n_o. The extraordinary axis n_e corresponds to $n_{\perp}$ and the ordinary axis n_o corresponds $n_{\parallel}$. The optical anisotropy or birefringence is given by the difference between the two indices of refraction; i.e. $\Delta n = n_{\parallel} - n_{\perp} = n_e - n_o$. A material is said to be positive uniaxial if optical anisotropy is positive (n_e is greater than n_o) and if the reverse exists, it is negative uniaxial.

The square root of the relative permittivities is equal to the two refractive indices of liquid crystals. Hence, $\mathbf{n}^2_{\parallel} - \mathbf{n}^2_{\perp}$ is related to the order parameter and can be used in estimation of the order parameter.[2]

1.5 Applications of LCs in designing biosensor

The properties of LCs make it a promising material for applications in biosensing. The surface anchoring of liquid crystals changes with respect to reorientations of liquid crystals due

to surface interactions and changes in surface topography. The elastic property of the LC allows the

surface interactions to be amplified as the surface interactions lead to change in ordering of mesogens in the bulk phase. This transition in orientation can be detected under polarising microscope as the LCs are birefringent.[11] Abott *et al* reported that changes in alignment of thin films of nematic LCs, prepared on a self assembled monolayer on anisotropic gold films, occur due to ligand binding events within the monolayer. [10] This publication inspired different groups to work on LC based sensing systems.

To study the interactions of different analytes, LCs can be confined to TEM grids kept on glass surfaces to make thin LC films. The surface of a glass slide is chemically treated to align the LCs on its surface. The films made are stable and prevents dewetting of the surface. It is usually coated with octadecyltrichlorosilane (OTS) or N,N-dimethyl-N-octadecyl-3 aminopropyltrimethoxysilyl chloride (DMOAP). When the TEM grid filled with LC is observed under the polarizing optical microscope, it gives a dark appearance indicating homeotropic anchoring. [12]

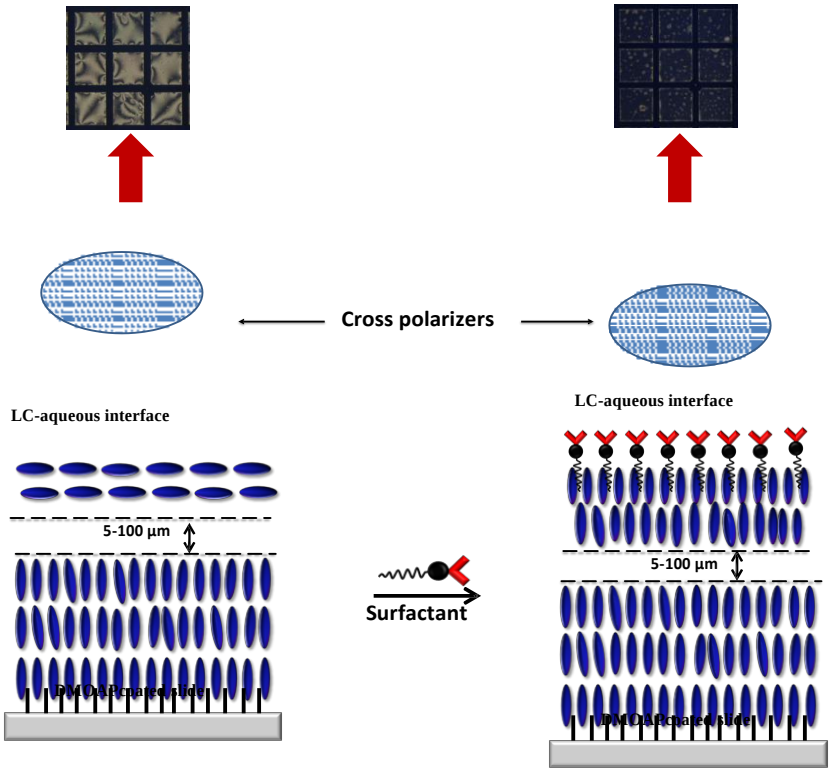

Figure 6: Illustration of LC film in aqueous medium showing bright optical appearance and LC film aligned by surfactants showing dark optical appearance under POM.

When immersed in an aqueous solution, the LCs has a planar orientation and appears bright under the polarizing optical microscope. The liquid crystals can be reoriented to homeotropic using surfactants through hydrophobic interaction of the liquid crystals with the long alkyl chain tails of the surfactants. This can be affected by concentration of surfactant, structure of the surfactant and length of the alkyl chain tail.[11]

The design of biosensors in LC systems is dependent on the change in its orientation as a result of the interaction of the analyte with the liquid crystals. Since there is a rigorous criterion for biosensors to be specific and selective to the analyte when it is present along with possible interferrants, the chemistry of the interaction taking place at the LC- aqueous interface must be considered carefully. In this project, we designed a sensor for dopamine using a boronic acid based amphiphile to align the LC film. The surface interaction probed was the formation of reversible covalent bond between the boronic acid based amphiphile and cis diol of dopamine. The nature of this cis diol interaction is not very specific, hence we have designed a system consisting of two point selective sites by exploiting the amine group of dopamine. This was linked with an amine selective crosslinker dithio(bissuccinimidylpropionate) which was functionalized on a gold nanoparticle.

1.6 Dopamine

Dopamine is a catecholamine neurotransmitter. It is synthesized from tyrosine which gets catalyzed by tyrosine hydrolase to form the precursor, L-dopa. L-dopa ,in turn, gets catalyzed by dopa decarboxylase, to form dopamine. It is secreted in the ventral tegmental area of the substantia nigra, midbrain and the arcuate nucleus of the hypothalamus. It plays an important role in emotional, pleasure and reward seeking behavior as well as learning, movement, stimuli responses and control of some endocrine glands.[13,14] Outside the central nervous system, dopamine is involved in vasodilation, diuresis and naturesis in the renal system and affects heart rate and heart muscles in the cardiovascular system. Dopamine has four major pathways:

Nigrostriatal, Mesolimbic, Mesocortical and Tuberoinfundibular. Each pathway is associated with different functions. As dopaminergic neurons are extensively found in the brain and is involved significantly in brain activity, an imbalance in the concentration of this neurotransmitter in the brain is associated with numerous mental disorders. Mental abnormalities

such as mood disorders, Parkinson's disease, Schizophrenia, substance addiction, Huntington disease, and

Attention Deficit Hyperactivity Syndrome (ADHD) are associated with dopamine level fluctuations.[15-20]

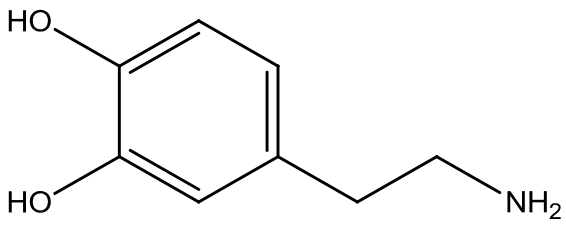

Figure 7: Structure of Dopamine

1.7 Interactions of Boronic Acids with cis diols

Boronic acids can form reversible covalent bonds with 1,2 and 1,3 cis diols to form five or six membered cyclic boronate esters or boronic esters depending on its pKa and pH of the media. In the biological system, diols are abundant and hence, diol-boronic acid interaction can be exploited to produce the recognition systems for diols and the design of various biosensors for molecules such as saccharides and catechols.[21-24] Selectivity in interaction of diol containing compounds with boronic acid is difficult to maintain, however, the interaction is of importance as it can form a stable covalent bond with the diol in aqueous media at physiological pH and thus, can be incorporated as one of the points of interaction in designing a selective system. The pK_a of boronic acid and the target molecule, pH of the reaction medium, dihedral angle of the diol can affect the boronic acid interactions.[25] So, a suitable buffer system and a boronic acid derivative soluble in aqueous media in physiological pH is required in which either the boronate anion or the boronic acid or both can can reversibly form covalent bonds to the cis-diol to generate a cyclic ester.

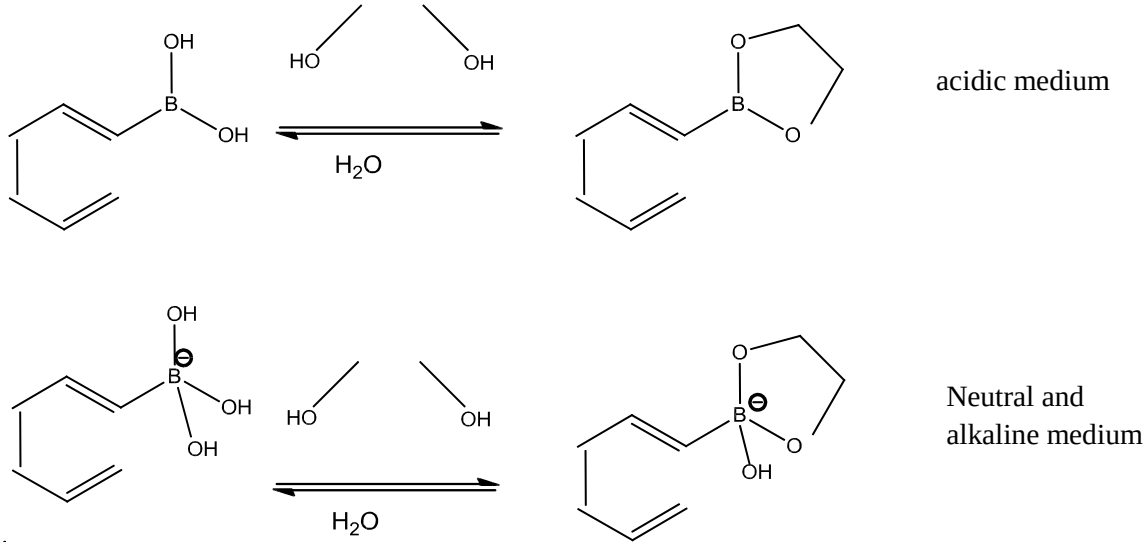

Figure 8: Reaction of Boronic acid with diols

1.8 Instumentation

1.8.1 Polarizing optical microscope (POM)

The polarizing optical microscope can be used to characterize and study the interactions of LCs due to their inherent birefringent property. The quantitative and qualitative analysis of the anisotropic specimens can be carried out. The microscope has a polarizer and an analyzer set at cross polars, that is 90 degrees relative to each other. The polarizer set vertically to the incident light allows only the entry of light polarized in the vertical direction which is then blocked by the analyzer resulting in dark appearance. However, in presence of an anisotropic sample, the plane polarized light from the polarizer interacts with the birefringent sample generating two components: ordinary and extraordinary rays which are oriented perpendicular to each other. When this light reaches the analyzer, the ordinary and extraordinary rays interact leading to constructive and destructive phases.

Dark optical appearance is observed when the light incident on the LC is polarized either perpendicular or parallel to the director, this light cannot pass through the analyzer as light is

polarized in only one direction and there is no component 90^0 to its direction. When an LC is observed under cross polars, the regions where the director orientation is not 0^0 or 90^0 to the polarization axis shows bright optical appearance. However, there is no preferred director orientation in the disclinations; and these areas appear as dark thread like appearance converging together.[3,2]

1.8.2 Raman Spectroscopy:

When light passes through a medium, there is a phenomenon of scattering of electromagnetic waves associated with it. The Rayleigh scattering occurs due to elastic collision of photons with the molecules. Here, the energy of scattered light is comparable to that of the incident light. Rayleigh scattering ceases to work when the size of the particle is greater than 10% of the incident wavelength but holds true for particles with dimensions lesser than the scattered wavelength. [26]

However, when the collision between the molecule and photons are inelastic, there is a change in energy of the scattered light as compared to the incident light. During inelastic collision, the molecule either receives or loses a part of its energy to the colliding photon. Thus, a change in energy observed corresponds to the energy gap between two quantum mechanically allowed states in vibrational, rotational or lower energy electronic transitions in molecular or atomic systems. The scattered radiation can either have a frequency lower (Stokes radiation) or higher (Anti-Stokes radiation) than incident radiation. Usually, Stokes radiation is more intense than Anti Stokes radiation[27]. Raman spectra considers the molecule as the scattering centre and does not depend on the wavelength of incident light.

Surface Enhanced Raman Spectroscopy (SERS)

SERS is an extension of Raman spectroscopy in which the Raman signals get enhanced by several orders of magnitude due to interaction of electromagnetic wave with metal surfaces. To measure a SERS spectra, a good probe is required. Usually, the probes are made of gold or silver as they can generate plasmon resonances in Vis-NIR region or have dimensions less than 100 nm.

Surface plasmons are delocalized electrons oscillating on a metal interface. SERS substrates are of three types: metal electrodes, metal coated planar surfaces or metal nanoparticles.[28]

Two mechanisms have been proposed for SERS:[28]

- The electromagnetic model proposes that when an incident electric field at a particular frequency strikes the metal surface, the localized surface plasmons get excited and resonates leading to increase in localized electromagnetic field. The result is an increase in Raman intensity.
- The charge transfer model states that a negatively charged excited molecule is formed when an electron, excited by incident radiation, interacts with an adsorbed molecule. The excited molecule undergoes nuclear relaxation to form a neutral molecule. The electron returns to the metal surfaces and results in the emission of a photon of different frequency.

Chapter 2

Experimental Methods

2.1 Materials used

Dopamine hydrochloride, Gold (III) chloride trihydrate, Sodium Citrate dihydrate, N,N- Dimethyl-N-octadecyl-3-aminopropyltrimethoxysilyl chloride (DMOAP), 5CB and PBS tablets (pH 7.4) were purchased from Sigma-Aldrich (St. Loius MO). Dithiobis(succinimidyl) propionate (DSP) was obtained from TCI. Sulfuric acid and hydrogen peroxide (30% w/v) were purchased from Merck. Ethanol was obtained from Jebsen & Jenssen GmbH and Co., Germany. Fischer's Finest Premium Grade glass slides were obtained from Fischer Scientific. Deionized distilled water was obtained using a Milli-Q-system (Millipore, bedford, MA). Gold specimen TEM grids (20 µm thickness,
50 µm wide bars, 283 µm,j grid spacing) were obtained from Electron Microscopy Sciences (Fort Washington, PA).

2.2 Methodologies

2.2.1 Synthesis of N-dodecylated 3-boronopyridinium bromide (1)

The amphiphile was synthesized as reported in published literature. [29] Dodecyl bromide (1.25 mM) and 3-N- boronopyridinium glycol ester (1mmol) were added into a roundbottom flask with acetonitrile as the solvent (40 mL). The reaction was refluxed at 73^0C and kept for 3 days. The product was washed using diethyl ether to remove unreacted reactants. The yellowish solid obtained was hydrolsed with a 1:9 mixture of aqueous sodium bicarbonate and dichloromethane for 1 day. The organic phase was removed and aqueous phase was extracted with excess of dichloromethane. The product was dried in vacuum and crystallized using ether.

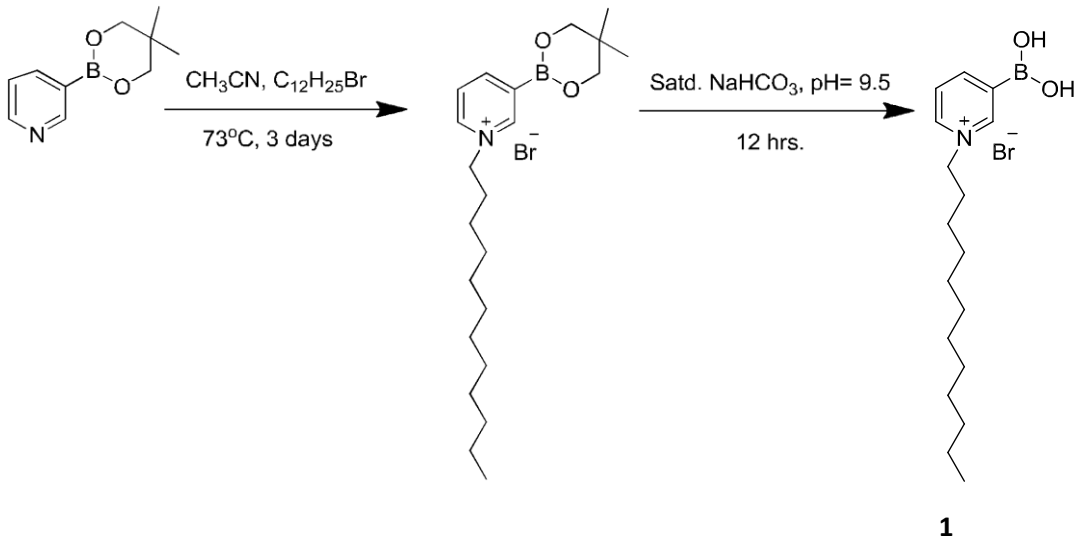

Scheme 2: Synthesis of N-dodecylated 3-boronopyridinium bromide (1)

2.2.2 Sample characterization for synthesized surfactant

A combined analysis using infrared spectroscopy (Perkin Elmer Spectrum Two), ^{1}H NMR (Bruker Biospin Switzerland Avance-iii 400 MHz), UV-vis-NIR spectrophotometers (Agilent Technologies, Cary 5000) and Mass spectrometry (Water Synapt G-2-s QTOF with MALDI ion source and α-cyano-4-hydroxy-cinnamic acid) was used to characterize the synthesized product.

^{1}H NMR spectra were recorded using tetramethylsilane as internal standard and deuterated chloroform as solvent ($CDCl_3$). The IR spectra were recorded by preparing a KBr pellet in neat form.

^{1}H NMR 400 MHz δ_H (ppm) 0.92 (s, 3H, CH_3), 1.21-1.41 (br s, 18H, $9CH_2$), 2.03-2.06 (m, 2H, NCH_2CH_2), 4.66 (t,2H, NCH_2CH_2); 8.13 (t, 1 H, Pyr-H_5), 8.61 (d, 1H, Pyr-H_4), 8.63 (s, 1H, Pyr-H_6), 9.05 (d, 1H, Pyr-H_2);

Tof MS m/z for $C_{17}H_{37}BNO_2$ (M-H calculated 370.1553) experimental 370.165

IR peaks (KBr pellet, νmax/cm^{-1}): 3407, 3054, 2924, 2854, 1634, 1487,1467, 1378, 1174, 1095, 770, 684, 415

2.2.3 Cleaning of glass slides

Piranha solution [70:30 (% v/v) H_2SO_4: H_2O_2(30%)] was used to clean the glass microscope slides. In a nutshell, glass slides were soaked in piranha solution maintained at 100°C for 1h ; followed by rinsing under running DI water for 5- 10 min. Then, the slides were further rinsed with ethanol thrice and dried under a stream of nitrogen. The cleaned slides were kept in an oven at 100°C overnight.

2.2.4 Preparation of DMOAP coated Glass Slides

The piranha cleaned glass slides were immersed in 0.1% (v/v) DMOAP solution in DI water for 30 min at room temperature and then, washed with DI water to remove unreacted DMOAP from the surface. The DMOAP coated glass slides were dried under a stream of nitrogen gas and kept in oven at 100ºC for 4 h to allow crosslinking of DMOAP.

2.2.5 Preparation of DSP functionalized gold nanoparticles

To prepare 13 nm citrate capped gold nanoparticle, 1 mM $HAuCl_4$ was made in 50 mL milliQ water and 5 mL of 38.8 mM sodium citrate was added to it. The mixture was heated on reflux for

30 minutes, cooled to room temperature and stored at 4˚ C.

To functionalize the gold nanoparticles, 4.72 µM of dithiobis(succinimidyl) propionate DSP was added to 5 mL of GNP solution and sonicated for 30 minutes.[30]

2.2.6 Preparation of Optical cells on TEM grids

The DMOAP coated glass slide was cut into small squares of dimensions 1 cm X 1 cm. A clean gold specimen grid was placed on the DMOAP coated glass piece and filled with approximately 0.2 µL of 5CB . The excess 5CB was removed using a syringe to generate a planar interface.

2.2.7 Optical Characterisation with Polarising Optical Microscope

The orientational transitions of LC in the sensing experiment were monitored using Zeiss Scope A.1 polarizing optical microscope at 5X magnification using cross polars. All images were captured with an exposure time of 80 ms. For investigation of 3D intensity

and grey scale of the images were processed to quantify the observations using Adobe photshop 7.0.

2.2.8 Measurement of UV-Vis spectra

The UV-Vis spectra of the surfactant, citrate capped GNPs, DSP functionalized GNP and dopamine were characterized using Cary 5000 UV-Vis- NIR spectrophotometer (Instrument Version 2.23) at room temperature. Phosphate buffer saline was used as a reference solution and a 1cm X 1cm sample cuvette was used.

2.2.9 Measurement of size using DLS

The size of nanoparticles were measured using Malvern Zetasizer Nano ZS90 instrument (Malvern Instruments, Southborough, Massachusetts) . The instrument was operated under 25^0C using a 632 nm and 4mW laser which is incident at 90^0 to the sample. The prepared samples were loaded into a glass cuvette and the reported values were quoted by taking an average of three successive measurements.

2.2.10 Measurement of Zeta Potential

Malvern Zetasizer Nano ZS90 instrument (Malvern Instruments, Southborough, Massachusetts) was used to measure the zeta potential. The instrument was operated under 25^0C and at an applied voltage of 100 V. For measurement of zeta potential, the samples were loaded in the zeta cuvette and zeta potential was recorded as an average of three successive measurements

2.2.11 Measurement of Raman Spectra

The Raman and SERS spectra were measured in RENISHAW Invia Microscope with a CCD detector. The measurements were taken with 514 nm laser with grating set at 1800 lines nm^{-1}. The sample was prepared by drop casting the solution on a clean glass slide and drying in air, In case of powdered samples, the samples were uniformly spread on the glass slide using a spatula before observing under the Raman microscope.

Chapter 3

Results and conclusions

3 .1 Characterisation of Gold nanoparticles

The gold nanoparticles were synthesized with citrate as the capping agent. The GNPs , thus synthesized, is observed to have a wine red colour and has a characteristic band at 522 nm corresponding to the surface plasmon resonance generated by them[29]. The concentration of the

GNPs was determined from its absorbance ($\varepsilon = 2.7 \times 10^8\ M^{-1}\ cm^{-1}$ at $\lambda = 520$ nm).[31] The GNPs were functionalized using dithiobis(succinimidylpropionate) (DSP). The UV spectra of the functionalized nanopaticles show no distinct change in peak position . The UV-Vis spectrum

of GNP and DSP-functionalized GNP is shown in Figure 9.

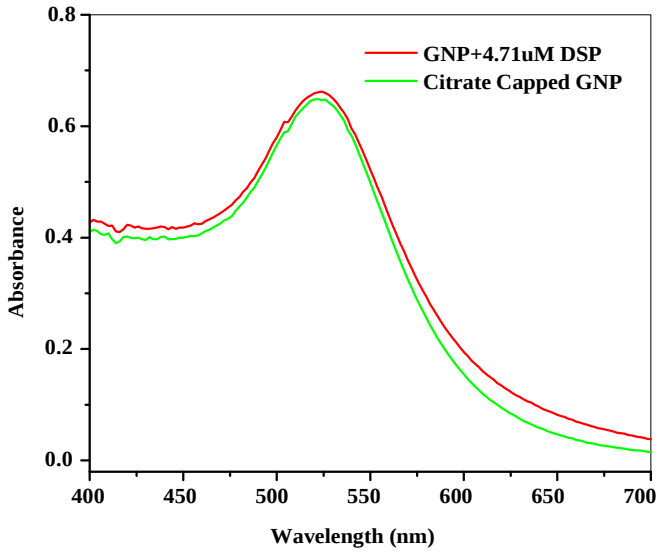

Figure 9: UV −Vis Spectra of GNP (green) and DSP functionalized GNP (red)

The size of the DSP functionalized gold nanoparticles were determined by dynamic light scattering (DLS). DLS measures the hydrodynamic diameter of a theoretical sphere which has mobility equal to that of the measured sample. The size measured by DLS can be influenced by substances adsorbed or bonded on the metallic core, and hence, can give a larger value.[32] The core diameter is assumed to be equal to the diameter of the sample as DSP is a small molecule. Measurements were carried out with water as dispersant at 25^0C temperature and refractive index

set at 1. 33. The z-diameter of the DSP functionalized GNP is determined to be 12.3 ± 0.1 nm. The uncertainty in measurement is expressed as the standard deviation.

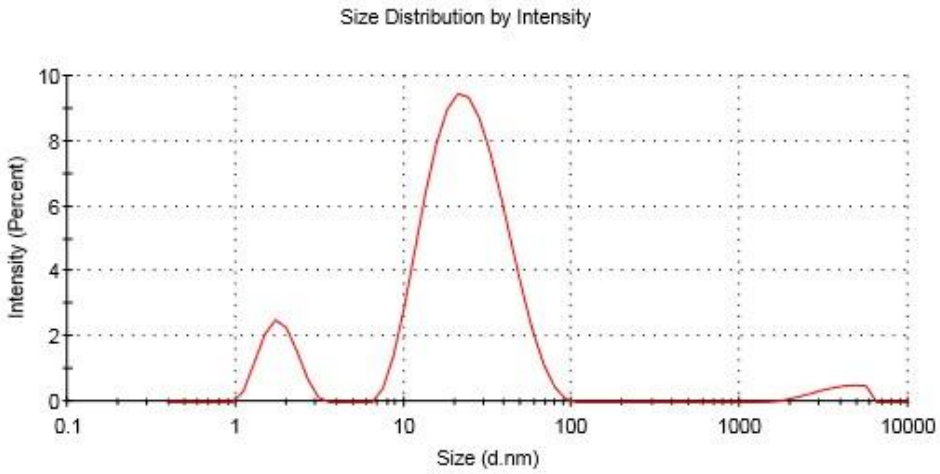

Figure 10: Size distribution by intensity plot of DSP functionalized GNP.

Zeta potential of citrate capped gold nanoparticles and DSP functionalized GNP was measured. DSP functionalized GNP shows an increase in zeta potential from -32.9 mV to -18.8 mV as compared to citrate capped GNPs. This can be possibly due to replacement of negatively charged citrate ions adsorbed on the surface of the metallic core by dithio(bissuccinimidylpropionate)
forming Au-S bonds on the surface.

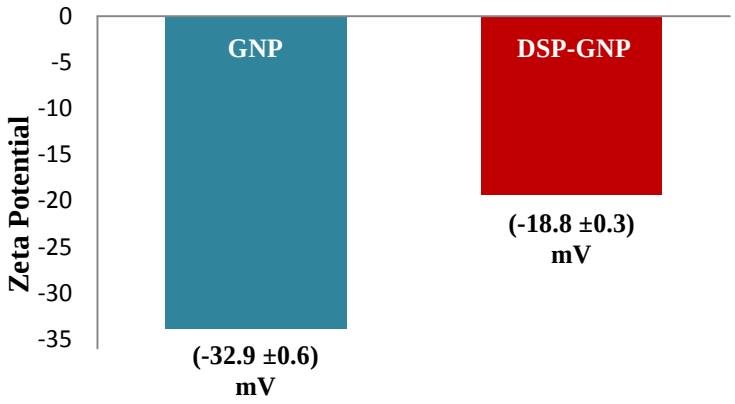

Figure 11: Zeta Potential of citrate capped GNP (green) and DSP functionalized GNP(red)

The functionalization of citrate capped GNPs by DSP was characterized by FT-IR. The samples were prepared by centrifuging about 3- 4 mL of the aqueous solution of citrate capped GNPs and DSP functionalized GNPs at 5000 rpm for about 15-20 minutes and suspending the precipitate in methanol after removing the supernatant. The sample was dried under high vacuum for about 10 hours in KBr. The IR spectra were recorded in neat form by preparing KBr pellets. The spectra were compared with that of sodium citrate and DSP.

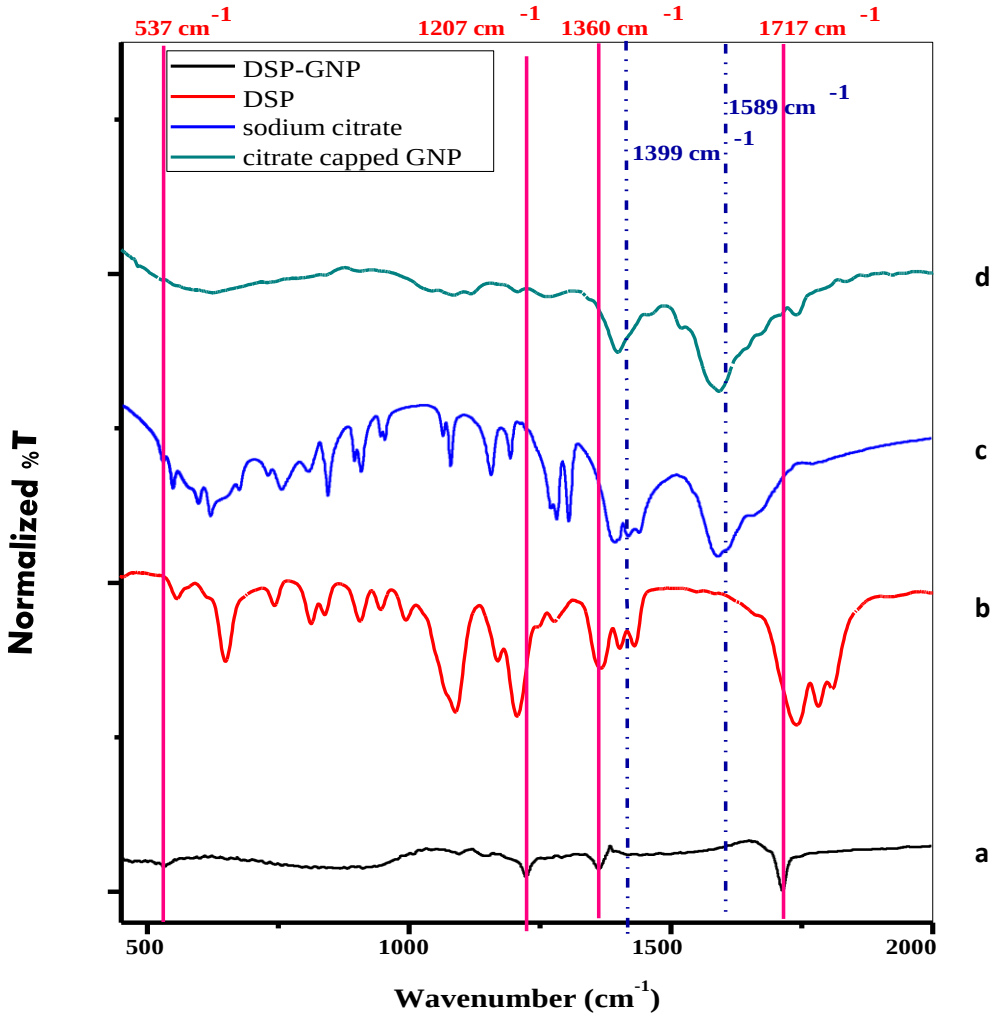

Figure 12: FTIR spectra of a) DSP functionalized GNP b) DSP c) Sodium citrate d) Citrate capped GNP recorded using in KBr pellet

Sodium citrate shows peaks corresponding to symmetric and asymmetric carboxylate groups at 1305-1415 cm^{-1} and 1500-1630 cm^{-1}. The peaks representing symmetric COO^- and asymmetric COO^- are at 1390 and 1591 cm^{-1} respectively (figure 12 c). This was compared to the spectra of vacuum dried citrate capped gold nanoparticles. The FT-IR spectra of citrate capped gold nanoparticle shows peaks coinciding with the asymmetric COO^- and symmetric COO^- at 1589 and 1399 cm^{-1} of citrate (figure 12 d). Hence, this shows the presence of citrate ions around the GNP.[33]

The peaks for DSP are assigned as: 558 cm^{-1} for C-S stretch, 1228 cm^{-1} and 1360 cm^{-1} for asymmetric and symmetric CNC stretch of NHS respectively and 1736 cm^{-1} for asymmetric C=O stretch of NHS (figure 12 b). On further comparing with the spectra of DSP functionalized GNP, we observe that the peaks of DSP are conserved in the spectral peaks of DSP functionalized

GNPs, although there is a slight shift in peak positions. The C-S stretch peak was shifted to lower wavenumber at 537 cm^{-1}, asymmetric CNC stretch of NHS was shifted to 1207 cm^{-1} and while symmetric CNC stretch of NHS was conserved at 1360 cm^{-1} and asymmetric C=O stretch of succinimidyl group was observed at 1717 cm^{-1} in case of DSP functionalized GNP (figure 12 a).[34] The FTIR spectra of DSP functionalized GNP shows almost no resemblance with the spectra of citrate capped GNPs as the free citrate ions were removed in the centrifugation step.

Hence, this gives the partial evidence of functionalization of GNP by DSP.

3.2 Analysis of POM Images

3.2.1 Optical Responses of surfactant aligned nematic LC 5CB in presence of dopamine

For our initial experiment, we aimed to study the effect of surfactant **1** on a 5CB film made on a TEM grid placed on a DMOAP coated glass slide in LC –aqueous interface. The LC film in contact with air interface remains in homeotropic orientation as the long hydrophobic chains of DMOAP aligns 5CB. On immersion in an aqueous media, the LC shows a transition to planar orientation resulting in a bright appearance under cross polars. The 5CB film immersed in PBS (phosphate buffer saline) buffer (pH 7.4) showed a bright appearance in POM.

The 5CB film was immersed in a solution of surfactant **1** made in 1mM PBS buffer (pH 7.4). The response of 5CB film to different concentrations of surfactant **1** was observed under cross polars. It has been previously reported that in a surfactant solution, the long chain hydrophobic tails of the surfactant align the liquid crystals to homeotropic orientation. From the POM images, we observe that a concentration of 10 μM shows a transition from black to bright appearance due to homeotropic alignment of 5CB in about 2 min while concentrations above 10 μM takes less than 2 minutes to align. Concentrations below 10 μM were also monitored and it was observed that takes longer time to align. Figure 13 show the cross polarized images of 5CB in a 10μM surfactant solution.

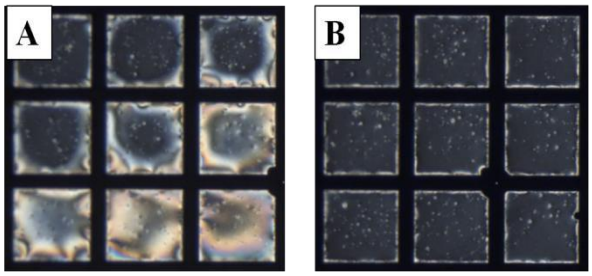

Figure 13: Cross polarized images of 5CB film in a 10 μM solution of surfactant **1** made in 1 mM PBS buffer (pH7.4) at A) 1 min and B) 2 min respectively (length of each square of the TEM grid = 283 μM)

Secondly, our goal is to analyze the optical responses of 5CB films in presence of surfactant **1** and dopamine inorder to design an LC based sensing system for dopamine. We have adopted a system in which 10 μM surfactant and different concentrations of dopamine in PBS buffer (pH

7.4) were incubated for a period of about 10 minutes. Then, a 5B film made on a TEM grid

placed on a DMOAP coated glass slide is immersed in the solution containing dopamine and surfactant and monitored under cross polars. We observe a transition from dark to bright patterns in the 5CB films. The detection limit was probed by monitoring varying

concentrations of dopamine. The images showing the response of 5CB to the presence of different concentrations of dopamine and 10μM surfactant after 60 minutes is shown in figure 14.We observed that small bright domains appear after about 5 to 10 minutes depending on the concentration of dopamine. A concentration of 100 μM dopamine shows the appearance of small bright domains; however, concentrations lower than 100 μM was unable to cause a transition from black to bright. Thus,

the system can detect a limiting concentration of 100 μM of dopamine. Past reports have shown that the cis-hydroxy groups form covalent interactions with boronic acid head groups.[21-24] From these results, we infer that the transition is possibly due to interaction of the cis-diol of dopamine with the boronic acid head group of surfactant **1**; causing a disruption in the alignment
of 5CB .

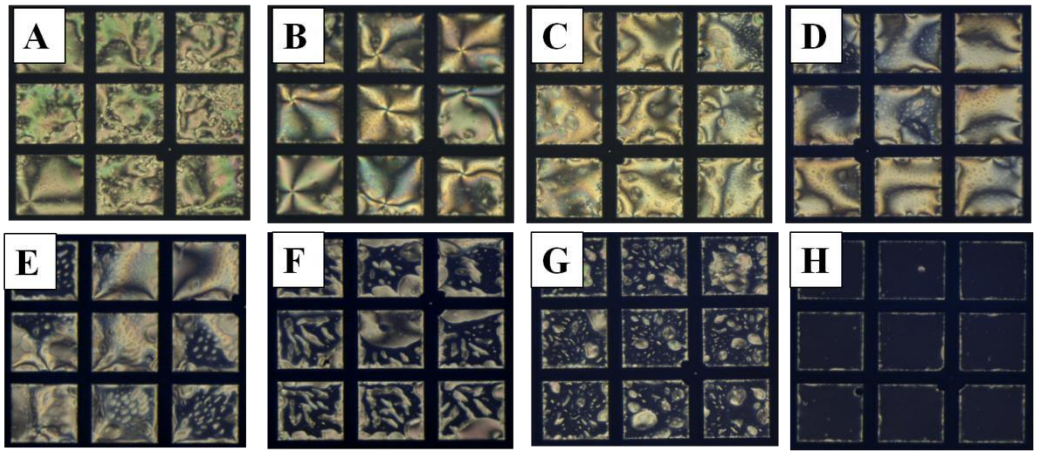

Figure 14: Cross polarized images of 5CB film in a 10 μM solution of surfactant **1** and dopamine prepared in 1 mM PBS buffer (pH 7.4) after 60 minutes for different concentrations of dopamine : A) 1 mM , B) 700 μM, C) 500 μM, D) 400 μM, E) 300 μM, F) 200 μM, G) 100 μM H) 50 μM. (length of each square of the TEM grid = 283 μM)

The change in optical response of LC was quantified by analyzing the change in grey scale intensity of images obtained after 60 minutes by using Adobe Photoshop 7.0. The grey scale intensity of the POM images was plotted against the concentration of dopamine (Figure 15). There is an increase in grey scale intensity till a concentration of 500 μM, after which it reaches saturation.

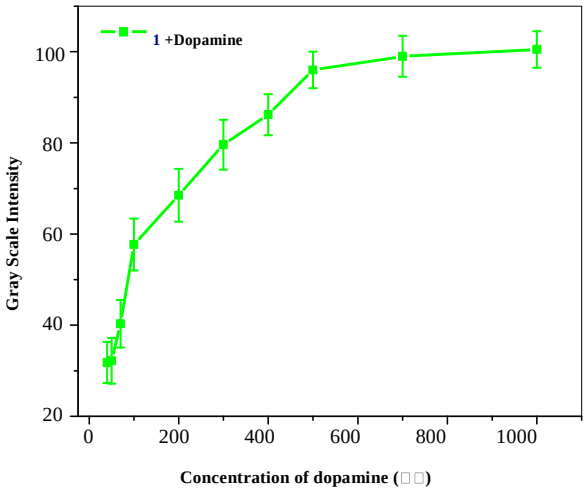

Figure 15: Plot of grey scale intensity against concentration of dopamine.

3.2.2 Variation in optical responses of surfactant aligned nematic LC 5CB in presence of DSP functionalized gold nanoparticles

In order to further lower the detection limit of dopamine in an LC system, we have designed a system using DSP functionalized gold nanoparticles. The approach, we have adopted, is to functionalize gold nanoparticles with DSP which acts as a stabilizer for the nanoparticles[30] and contains an amine reactive succinimidyl moiety which can react with the amine group present in dopamine while the cis-diol of dopamine interacts with the boronic acid head group of the surfactant **1**.

We have performed a control experiment to determine the concentration of functionalized GNP required for our experiment. In a solution of 10 μM surfactant, we added different concentrations of functionalized GNPs and monitored the response. It was observed that a concentration of 0.14 nM does not interfere with the optical transition of surfactant from bright to dark (Figure 16).

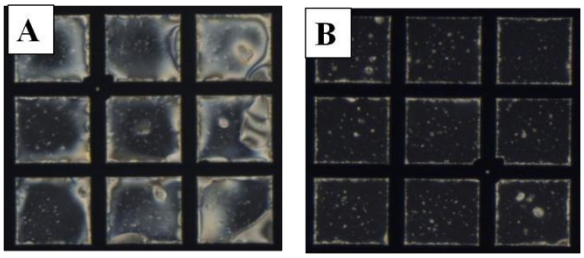

Figure 16: Cross polarized images of 5CB film in a 10 μM solution of surfactant **1** and 0.14 nM DSP functionalized GNP made in 1 mM PBS buffer (pH 7.4) at A) 1 min and B) 2 min respectively (length of each square of the TEM grid = 283 μM)

Further, we proceeded to monitor the system of surfactant **1** and dopamine in presence of DSP functionalized GNP. We incubated the solution of dopamine and 10μM surfactant for 10 minutes, this is followed by incubation of this system with 0.14 nM of DSP functionalized GNP for 10 minutes. We adopted this order of addition inorder to promote the complexation of dopamine and surfactant head group; followed by the reaction of N-hydrosuccinamide ester (NHS) end group of DSP to the amine moiety of dopamine.

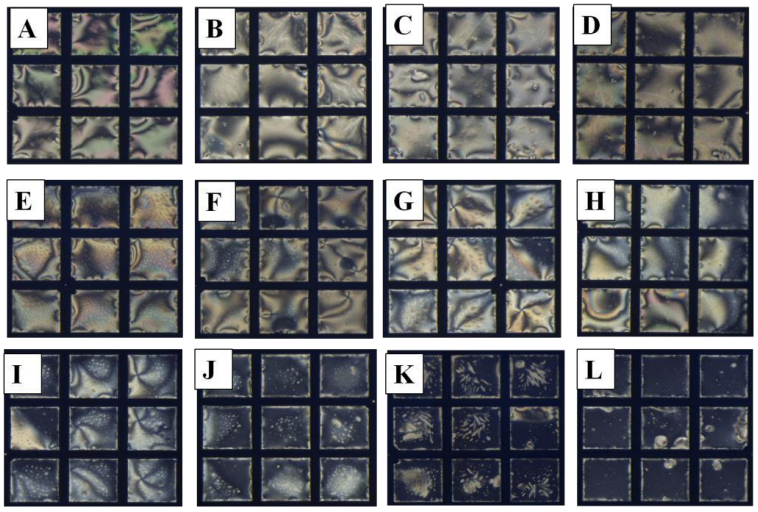

Figure 17: Cross polarized images of 5CB film in a 10 μM solution of surfactant **1** and dopamine with 0.14 nM DSP functionalized GNP prepared in 1 mM PBS buffer (pH 7.4) after

60 minutes for different concentrations of dopamine : A) 1 mM , B) 500 μM, C) 300 μM, D) 100 μM, E) 50 μM, F) 30 μM, G) 10 μM, H) 1 μM , I) 0.7 μM, J) 0.5 μM, K) 0.3 μM and L) 0.1 μM (length of each square of the TEM grid = 283 μM).

The POM images (Figure 17) shows the response of the system with varying concentrations of Dopamine. The transition from dark to bright can take between 10 to 60 minutes depending on the concentration of dopamine. We can infer that the detection limit of dopamine is substantially reduced from 100 μM in absence of nanoparticle to 0.3 μM. This may be attributed to greater disruption of 5CB by the complex formed by surfactant **1** and dopamine bound to the GNP.

The grey scale intensity plot against concentration of dopamine in this system shows a steeper rise as compared to the system in absence of dopamine reaching asaturation at 100 μM. This
shows that the system shows greater response in presence of DSP functionalized GNP.

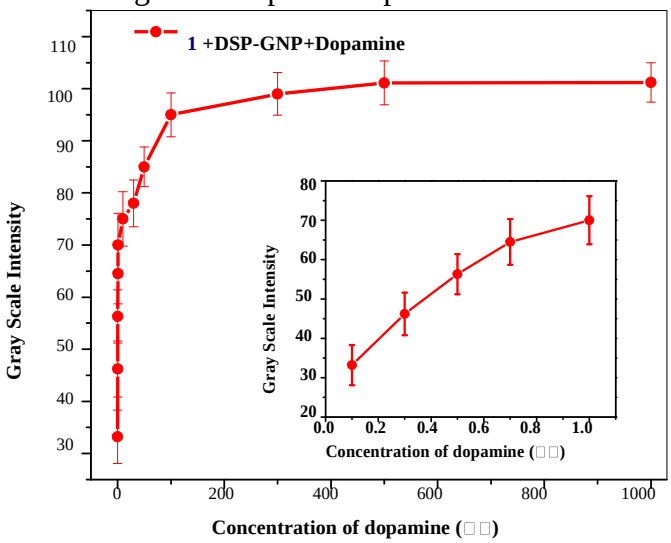

Figure 18: Plot of grey scale intensity against concentration of dopamine in presence of DSP functionalized GNP.

3.2.3 Selectivity

The design of a sensitive and selective system for dopamine based on the covalent interaction with boronic acid derivatives is hindered by the presence of different diols and catecholamine derivatives present in biological system. We have selected tyramine, serotonin, epinephrine and nor epinephrine as they can potentially induce similar interactions as dopamine on account of their similar structure.The structures of the selected compounds are shown in figure 19.

The solutions of these compounds were incubated for about ten minutes with 10 μM of surfactant **1**

0.14 nM of DSP functionalized GNPs was added to this system and incubated for 10 min.

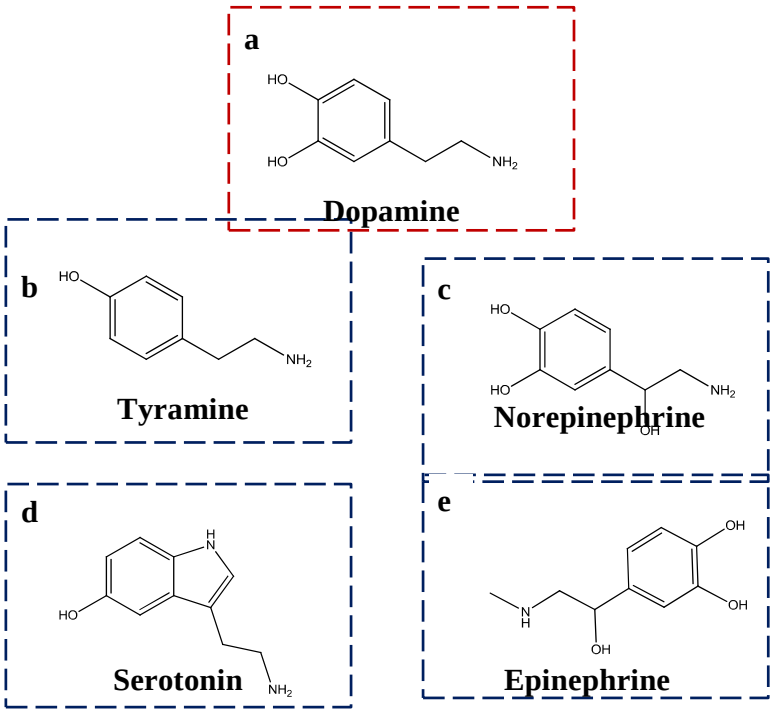

Figure 19: Chemical structures of a) Dopamine, b) Tyramine, c) Norepinephrine, d) Serotonin and e) Epinephrine

The POM micrographs (figure 20) shows that Tyramine and Epinephrine are unable to cause a transition in alignment of 5CB on the TEM grids when exposed to concentrations upto 0.5 mM. While norepinephrine and serotonin induced a tilted orientation of 5CB for a concentration till 0.3 mM after a period of 60 minutes. However, dopamine is more sensitive to the system as the time taken and the concentration required to induce a transition is lower as compared to that of norepinephrine and serotonin.

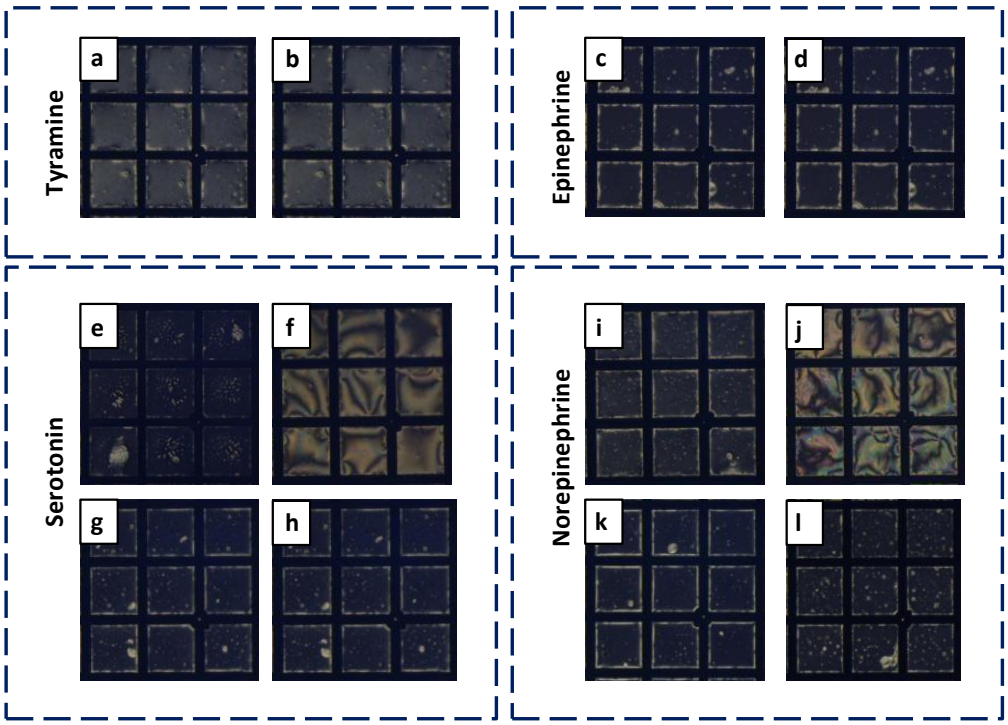

Figure 20: Polarized optical microscope images in at 10 minutes and 60 minutes respectively: 0.5 mM Tyramine (a,b); 0.5 mM Epinephrine (c,d); 0.3 mM Serotonin (e,f) and 0.2 mM Serotonin (g,h); 0.3 mM Norepinephrine (i,j) and 0.2 mM Norepinephrine (k,l) in solution of 10 μM surfactant 1, 0.14 nM DSP functionalized GNP made in 1 mM PBS buffer (length of each square in the TEM grid = 283 μM)

On comparing the polarized optical micrographs, it is observed that dopamine is able to change the surfactant aligned 5CB , as evident from the transition from dark appearance to bright textures, within 10 to 60 minutes for similar concentrations , but no such response was observed in case of the compounds selected for this study. Hence, the system can selectively detect dopamine over other possible competitors.

3.3 Stability of complex monitored through UV-Vis Spectroscopy

The stability of the complex of surfactant **1**, dopamine and DSP functionalized GNPs were further analyzed by UV-Vis Spectroscopy. On analyzing the UV-Vis spectra of surfactant dopamine complex, we find that the peaks corresponding to dopamine at ~258 nm and ~265 nm and surfactant at ~281 nm (figure 21 A) were conserved in the spectra of the complex; (figure 21

B). The solution of dopamine and surfactant were monitored over time; and it was observed that the intensity of peaks showed no significant change over 60 minutes.

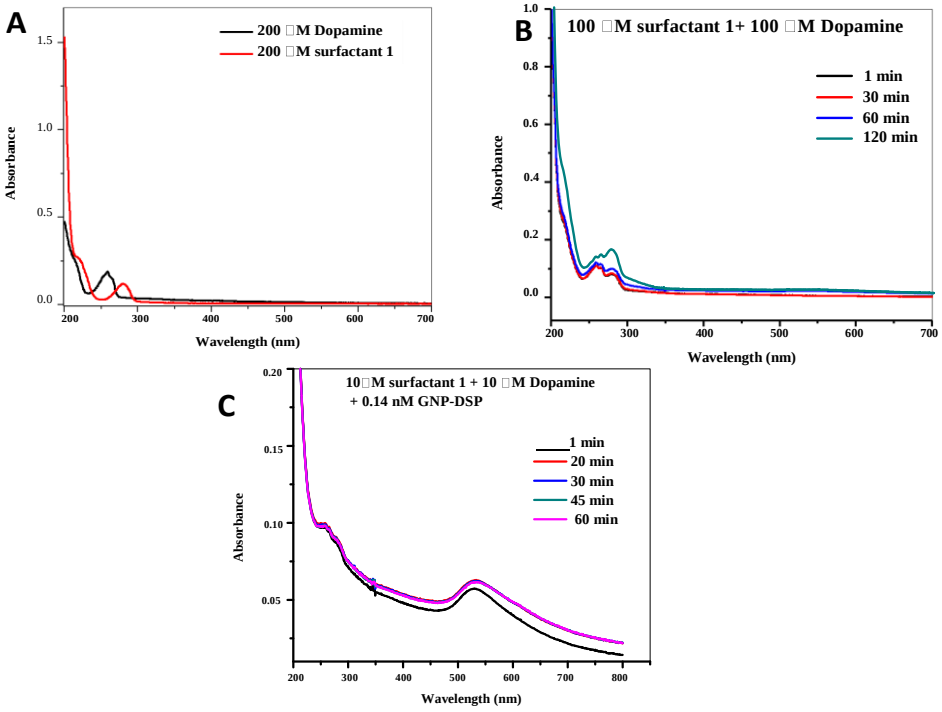

Figure 21: UV-Vis spectra of A) 200 µM Dopamine (red) and 200 µM surfactant **1** (black) B) 100 µM Dopamine +100 µM surfactant **1** monitored over 120 minutes C) 100 µM Dopamine + 100 µM surfactant **1** in presence of 0.14 nM DSP functionalized GNP monitored over 60 minutes

We monitored the solution of surfactant **1** and dopamine in presence of DSP functionalized GNP. The spectra shows an absorption band corresponding to surface plasmon resonance which is much stronger than the other absorption bands corresponding to the surfactant-dopamine complex. The absorption band for the dopamine–surfactant complex shows no detectable change.

However; the surface plasmon band which arises due to the GNP shows a shift in position from ~522 nm for only gold nanoparticle (figure 9) to ~529 nm in the sample. The shift in surface plasmon band is likely due to change in dielectric constant of the nanoparticle due to adsorption of analytes. The sample was monitored over a period of 60 minutes, we find that the intensity of

peaks increased after 20 minutes as compared to the first minute. The intensity of peaks remains constant till 60 minutes indicating the stability of the complex.

3.4 FT-IR spectral Studies

To probe the formation of the complex, we recorded the FT-IR spectra of the complexes in neat form. Two samples were prepared by incubating 1:1 weight ratio of dopamine and 3- Pyridinium boronic acid (3PBA) and 1:1:1 weight ratio of 3-PBA, dopamine and DSP in a mixture of 2 parts CH_3OH and 1 part DCM and dried. The peaks in the resulting spectra were compared with that of dopamine, 3 PBA and DSP (figure 22).

Boronate ester:

To confirm the formation of boronate ester, we analyze the fingerprint region of IR spectra as the hydroxyl peaks of the 3-PBA (3639-3634 cm^{-1}) still persists due to presence of unreacted catechol or boronic acid and hence, is not indicative of formation of the cyclic boronate ester. On comparing the different spectra (figure 22), we observed that there shift in peak positions in the spectra of 3-PBA with dopamine without DSP (figure 22 b) and with DSP (figure 22 c) from that of 3- PBA (figure 22 a). The two spectra show 4 new peak positions: the peak at 688 cm^{-1} corresponds to out of plane vibrational modes of boron syn to the out of plane displacements of aryl hydrogen atoms. In the higher frequency range, the breathing mode of the C_2 O_2B ring which is due to the lengthening of B-C and shortening of C=C bonds and vice versa in the ring gives rise to a peak at 1443 cm^{-1}. The 1263 cm^{-1} vibrational peak is due to symmetric lengthening or shortening of B-C and C=C bonds. Further, the peak at 1247 cm^{-1} is due to C-O stretching in the 5 membered cyclic boronate ester ring symmetrically.[35]

Formation of amide bond:

The spectrum of 3-PBA-dopamine-DSP sample does not show much resemblance with either dopamine or DSP. The peak of dopamine at 1500 cm^{-1} gets higher shifted to 1492 cm^{-1}which correlates to N-H amide stretch. The peak of DSP at 1742 cm^{-1} gets lower shifted to 1703 cm^{-1}.

The peak at 1703 cm^{-1} is indicative of the formation of an amide C=O stretch.

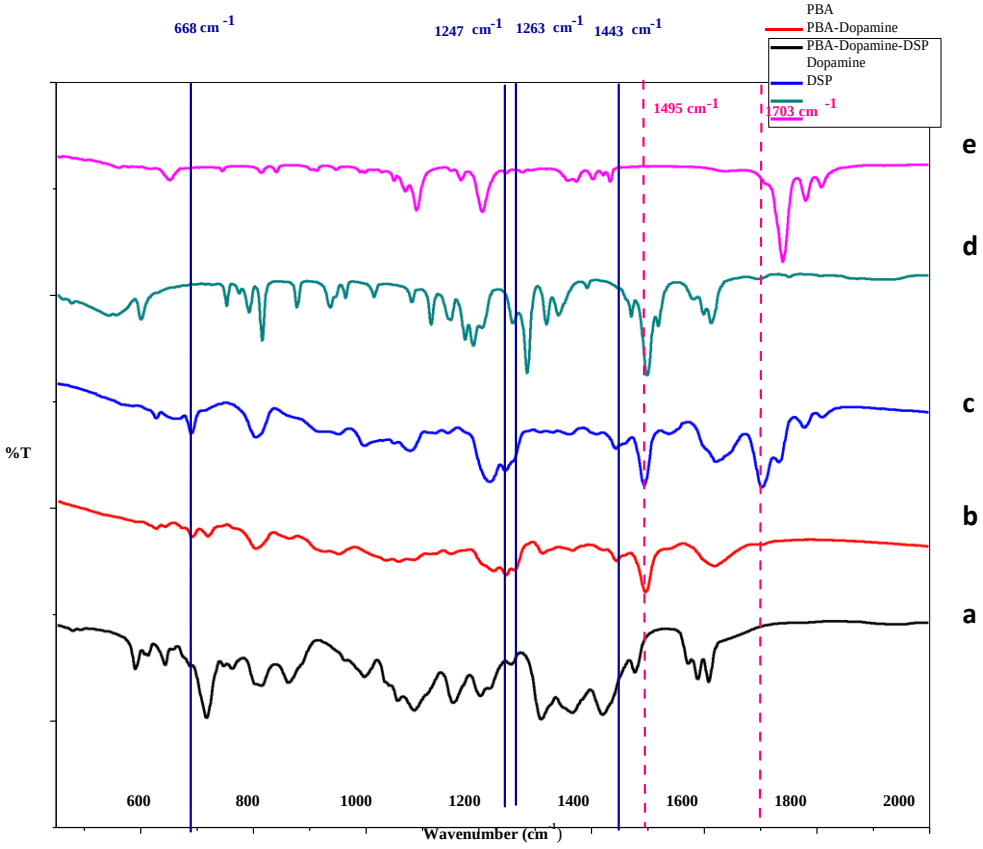

Figure 22: FTIR spectra of a) 3- Pyridinium boronic acid b) 1:1 ratio (by wt.) of 3-Pyridinium boronic Acid and dopamine c) 1:1:1 ratio (by wt.) of 3-Pyridinium boronic Acid and dopamine and DSP d) Dopamine e) DSP

3.5 Raman studies

The SERS spectra of the complex of the surfactant **1** with dopamine and DSP functionalized

GNP was recorded to further probe the interactions. A solution of 100 µM surfactant and 100 µM dopamine was made with DSP functionalized GNP. The solution was drop casted on a glass slide. This spectra was compared with the Raman spectra of dopamine powder, The dopamine powder showed characteristic peaks at 592, 627, 750, 790, 944,1113, 1145, 1285,1317 and 1616 cm^{-1}.[36] The SERS spectra of the complex showed the intensity reduction of the 750 and 790 cm^{-1} peaks while there is a shift in peak positions in case of others. This can possibly due to formation quinone form of dopamine[35] or due to cyclic ring formation of boronate ester .

Additional peaks appear at 1495 cm^{-1} corresponding to the C=C aromatic stretching of dopamine,[37] the peak at 1587 cm^{-1} can be attributed to aromatic ring of boronic acid. [38] The formation of a complex between the DSP functionalized gold nanoparticle and amine of dopamine can be inferred from the appearance from a faint band at 1637 cm^{-1} (amide region).[39] Therefore, the SERS spectra gives an evidence for the formation of the complex.

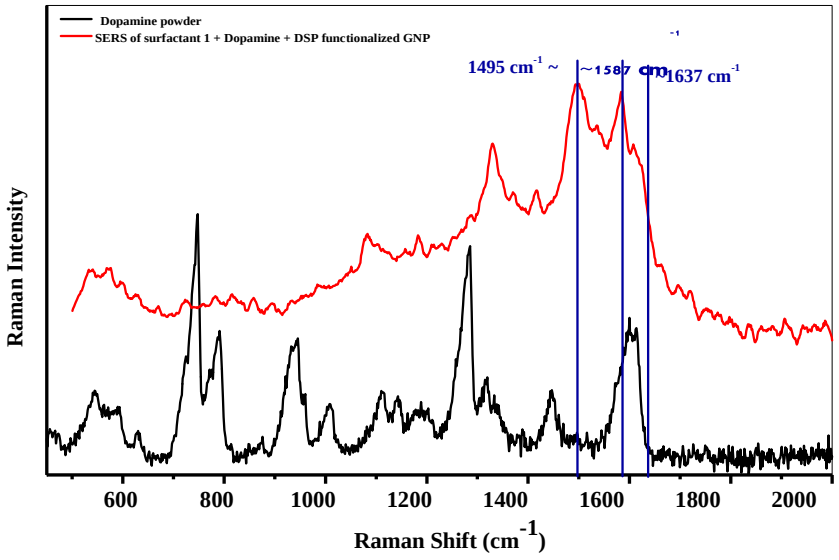

Figure 23: Raman spectra of Dopamine powder (black) and SERS spectra of complex of Surfactant 1a-Dopamine and DSP functionalized GNP

3.6 Conclusions

To summarise this work, we synthesized a boronic acid based amphiphile in which the head group can interact with cis diols to form a cyclic ester along chain tails can align liquid crystals in LC aqueous interface. We designed an LC based sensor system for dopamine which has two points of interaction: the boronic acid head group forms a covalent cyclic boronate ester while the amine moiety of dopamine reacts with the amine reactive crosslinker DSP functionalized on a gold nanoparticle. Incorporating DSP functionalised GNP in the system increased the limit of detection from 100 µM to 0.3 µM. The detection of dopamine with DSP −GNP shows faster transition and has lower LOD than molecules with similar structure. The formation of the complex was confirmed through FTIR and Raman studies. And the system was found to be selective for dopamine as compared to other possible interferences.

3.7 Future outlook

The real time detection of the analyte needs to be carried out using samples in cerebrospinal fluid or human serum.

Bibliography

1. de Gennes, P. G.; Prost, J. *The physics of liquid crystals*, Oxford University Press, **1994**.
2. Collings, P. J.; Hird, M. *Introduction to Liquid Crystals Chemistry and Physics*, Taylor & Francis: London, **1997**.
3. Collings, P. J. *Liquid crystals: nature's delicate phase of matter*, Princeton University Press, **2002**.
4. Priestley, E. B.;Wojtowicz, P.J.;Sheng,P. *Introduction to Liquid Crystals* Plenum Publishing Corporation, New York **1975**
5. Kumar, S. *Chemistry of Discotic Liquid Crystals: From monomers to polymers*, Taylor and Francis Group, **2011**
6. Michael, J.; Stephen Straley, J.P . *Reviews of Modern Physics*. **1974**, 46 (4), 617
7. Lockwood, N.A.; Gupta, J.K.; Abbott; N.L. *Surface Science Reports* . **2008**, 63, 255.
8. Bai,Y. and Abbott, N.L. *Langmuir.* **2011**, 27, 5719.
9. Lowe, A.M. and Abbott,N.L *Chem. Mater.* **2012**, 24, 746.
10. Gupta,V.K.; Skaife, J.J; Dubrovsky,T.B.; Abbott, N.L. *Science*. **1998**, 279, 2077.
11. Brake, J.M., Mezera, A.D., Abott, N.L. *Langmuir.* **2003**, 19, 6346.
12. Brake, J.M. ; Abott , N.L. *Langmuir* **2002,** *18,* 6101.
13. Brooks, D.J. *J. Neural Transm.* **2001**, 108, 1283.
14. Wise, R.A. *Nature Reviews Neuroscience*. **2004,** 5 , doi:10.1038/nrn1406
15. Volkow, ND Fowler, JS ;Wang, G-J and Swanson, J.M. *Molecular Psychiatry.* **2004,** 9, 557.
16. Volkow, ND ; Wang, G-J ; Newcorn, JH ; Kollins, SH ; Wigal, TL; Telang,F; Fowler, JS ; Goldstein, RZ ; Klein, N; Logan, J; Wong, C and Swanson; JM *Molecular Psychiatry* **2011,** 16, 1147.
17. Kim,J-H; Auerbach, JM; Rodrı´guez-Go´mez,J A; Velasco, I; Gavin, D; Lumelsky, N.; Lee, S-H; Nguyen, J; Sa´ nchez-Pernaute, R; Bankiewicz, K. & McKay, R. *Nature* **2002**, 8, 50.
18. Russo, S. J. and Nestler E. J. *Nat. Rev. Neuro.* **2015,** 14, 609.
19. Howes , O.D. and Kapur, S. *Schizophr . bull.* **2009,** 35 (3) , 549.

20. Ayano, G**.**, *J Ment Disord Treat* **2016**, 2:2 doi: 10.4172/2471-271X.1000120.
21. Wu,X; Chena, X-X and Jiang, Y-B *Analyst.* **2017**, 142, 1403.
22. P˘ribyl, J. and Skl´adal, P. *Analytica Chimica Acta.* **2005** , 530 ,75.
23. Yan-Jun Huang, Y-J; Jiang,Y-B; Fossey, J.S.; James, T.D. and Marken, F *J. Mater. Chem*., **2010**, 20, 8305.
24. . Bull,S.D.; Davidson, M.D.;Van Dan Elsen, J.M.H; Fossey, J.S.; Jenkins,T.A. ; Jiang, Y-B; Kubo, Y; Marken, F; Sakurai,K.; Zhao, J. and James, T.D. *Acc. Chem. Res*., **2013** 46 (2), 312.
25. Yan,J; Springsteen,G. ; Deeter, S. and Wang,B. *Tetrahedron* **2004**, 60, 11205.
26. Y. Harada and T. Asakura, *Radiation forces on a dielectric sphere in the Rayleigh scattering regime*, Optics Communications. **1996**, 124,529.
27. Banwell, C.N. ; McCash , E.M. *Fundamentals of Molecular Spectroscopy* , Tata McGraw Hill, UK, **2011.**
28. Ru, E.L. ; Etchegoin, P. *Principles of Surface Enhanced Raman Spectroscopy and related plasmonic methods* , Elsevier, **2009.**
29. Karpichev, Matondo, H.; Kapitanov, I.; Savsunenko, O.; Vendrenne, M.; Poinsot, V. and Rico –Lattes, I.; Lattes, A. *Cent. Eur. J. Chem.* **2012**, 10(4), 1059-1065
30. Kong, B.; Zhu,A.; Luo,Y.; Tian,Y.; Yu,Y. and Shi,G. *Angew. Chem. Int. Ed.* **2011**, 50, 1837.
31. Huo, F.; Lytton-Jean, A. K. R. and Mirkin, C. A. ; *Adv. Mater.* **2006**, 18, 2304.
32. Zheng, T.; Bott, S. and Huo **,** Q. *ACS Appl. Mater. Interfaces*. **2016**, *8* (33), 21585.
33. Park,J-W; Parry, J.S.S. *J.Am.Chem.Soc*. **2014**,136.1907.
34. Lim, C.Y.; Owens, N.A.; Wampler, R.D.; Ying, Y., Granger, J.H. and Porter, M.D. *Langmuir*. **2014**; 30(43): 12868.
35. Smith, M.K.; Northrop, B.H. *Chem. Mater.* **2014**,26, 3781
36. G. John D. Ciubuc, G.J.D.; Bennet, K.E.; Qiu, C. Alonzo, M.; William G. Durrer, W.G.; and Manciu, F.C. *Biosensors.* **2017**, 7, 43 doi:10.3390/bios7040043
37. Wang,P.; Xia, M.; Liang,O ; Sun,K.; Cipriano,A.F.; Schroeder,T.; Liu,H. and Xie, Y.H. *Anal. Chem.* **2015**, 87, 10255

38. Li,S, ; Zhou, Q.; Chu, W.; Zhao, W. and Zheng, J. *Phys. Chem. Chem Phys*. 2**015**, 17, 17638
39. Peaks were assigned from the Raman correlation table downloaded from http://www.utsc.utoronto.ca/~traceslab/raman%20correlation%20table.pdf